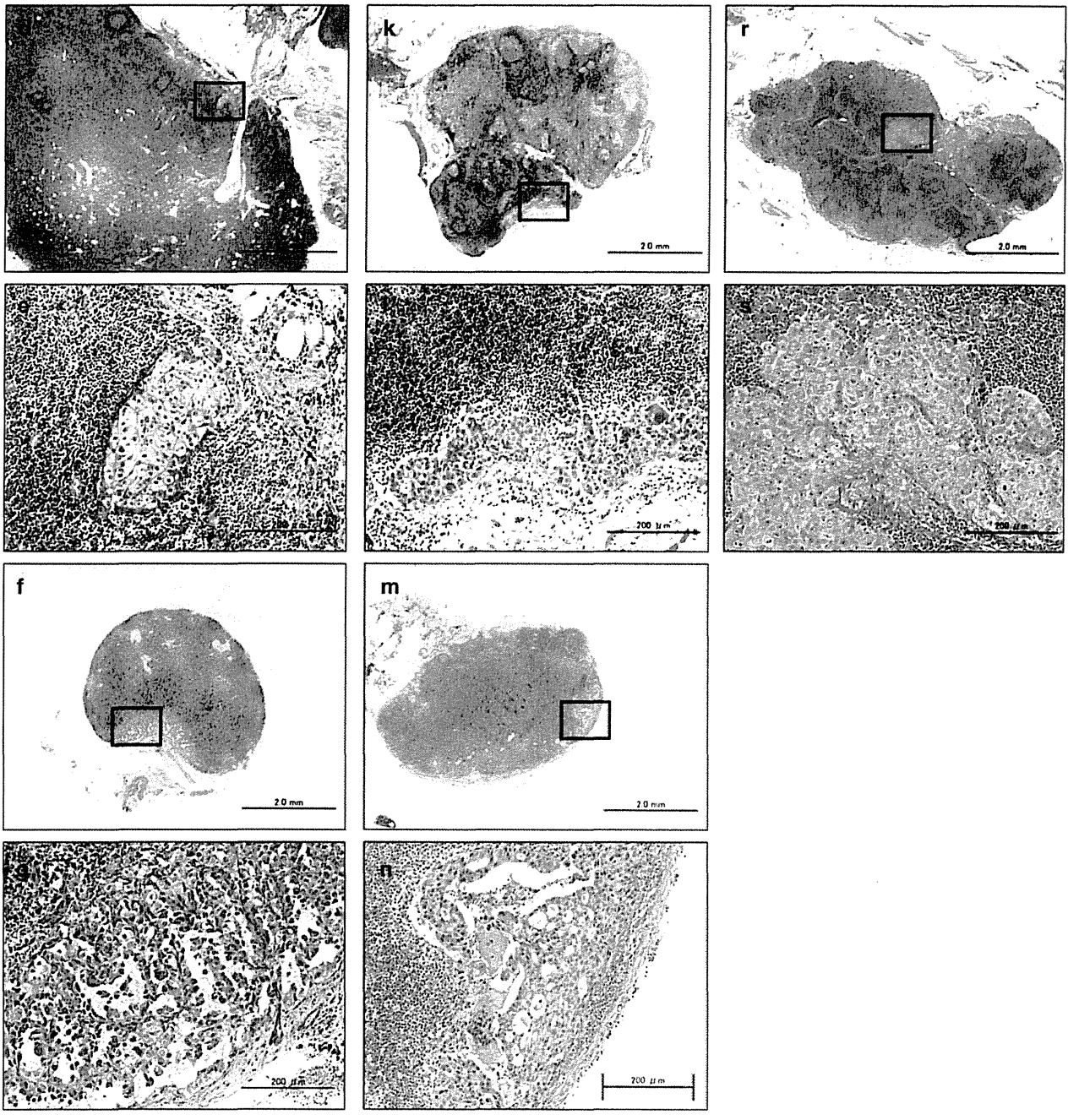

Figure 1 Continued

are summarized in Table 1. In all, 54 patients (33.1%) and 109 patients (66.9%) were pathologically diagnosed as belonging to the N1 and N2 categories, respectively.

The histologic subtypes of the primary tumors were distributed as follows: lepidic-predominant subtype, 6 tumors (3.7%); papillary-predominant subtype, 59 tumors (36.2%); acinar-predominant subtype, 35 tumors (21.5%); solid-predominant subtype, 63 tumors (38.6%).

Pathological characteristics of the metastatic lymph node tumors

Clinicopathological information pertaining to the 509 metastatic lymph node tumors is summarized in Table 2. In all, 286 (56.2%) and 223 (43.8%) of the metastatic lymph node tumors were pathologically diagnosed as belonging to the N1 region and N2 region, respectively. The histologic subtypes

Table 1 Characteristics of the patients with lymph node metastasis

Factors	$n = 163$ (%)
Age (years)	
<65	71 (43.6)
≥65	92 (56.4)
Sex	
Male	100 (61.3)
Female	63 (38.7)
Smoking history	
Never smoker	59 (36.2)
Current/Previous smoker	104 (63.8)
Pathological T classification	
pT1	40 (24.5)
pT2	81 (49.7)
pT3	33 (20.3)
pT4	9 (5.5)
Pathological N classification	
pN1	54 (33.1)
pN2	109 (66.9)
Pathological Stage (UICC7)	
Stage IIA	34 (20.8)
Stage IIB	6 (3.7)
Stage IIIA	111 (68.1)
Stage IIIB	7 (4.3)
Stage IV	5 (3.1)
Predominant subtype in primary tumor	
Lepidic	6 (3.7)
Papillary	59 (36.2)
Acinar	35 (21.5)
Solid	63 (38.6)
Number of metastatic lymph nodes	
1	47 (28.8)
2–5	82 (50.3)
≥6	34 (20.9)

Table 2 Characteristics of metastatic lymph node tumors

Factors	$n = 509$ (%)
Region	
Hilar, lobar and segmental (N1)	286 (56.2)
Mediastinal (N2)	223 (43.8)
Predominant subtype	
Papillary	107 (21.0)
Acinar	119 (23.4)
Solid	283 (55.6)
Metastatic lesion size	
≤2 mm	122 (24.0)
>2 mm, ≤5 mm	165 (32.4)
>5 mm	222 (43.6)

of the metastatic lymph node tumors were distributed as follows: papillary-predominant subtype, 107 lymph nodes (21.0%); acinar-predominant subtype, 119 lymph nodes (23.4%); solid-predominant subtype, 283 lymph nodes (55.6%).

Size distribution of the metastatic lymph node tumors

The median diameter of the lesions was 5 mm. The numbers of metastatic lymph node tumors belonging to the three size categories of ≤2 mm, >2 mm but ≤5 mm (median size) and >5 mm were 122 (24.0%), 165 (32.4%) and 222 (43.6%)(Table 2).

The number of histologic subtypes in the metastatic lymph node tumors divided according to the size

We compared the number of component histological subtypes in the primary tumors and metastatic lymph node tumors by dichotomizing the metastases according to the tumor diameter into ≤2 mm or >2 mm. The number of subtypes in the metastatic lymph node tumors in the group in which the primary tumor was composed of one subtype was 1.00 ± 0, indicating that all metastatic tumors arising from primary lesions composed of a single histologic subtype also showed a single histologic subtype (Fig. 2a). Fig. 2(b–d) shows the comparisons between the two metastatic tumor groups (divided according to the tumor size) in each case of the primary tumor being composed of two, three, or four subtypes, respectively. No significant differences between the two size groups were observed in the metastatic tumors arising from primary tumors composed of two histologic subtypes. On the other hand, significant differences between the two size groups were observed in the metastatic tumors arising from primary tumors composed of three or four subtypes (Fig. 2c,d; $P < 0.01$ and $P < 0.01$). The mean numbers ± standard error (SE) of subtypes in the metastatic lymph node tumors that were ≤2 mm and >2 mm in diameter were 1.18 ± 0.06 and 1.60 ± 0.05, respectively, and 1.32 ± 0.11 and 1.75 ± 0.06, respectively.

Comparison between the predominant histologic subtypes in the primary tumors and metastatic lymph node tumors

We compared the predominant histologic subtypes of the primary tumors and 509 metastatic lymph node tumors (Table 3). The predominant subtypes of the metastatic lymph node tumors in the cases in which the primary tumors showed the lepidic-predominant subtype were the papillary subtype (50.0%) and acinar (50.0%) subtype. The predominant subtype of the metastatic tumors in the cases in which the primary tumors showed the papillary-predominant subtype was the original papillary subtype (47.4%), followed by the solid (39.7%) and acinar (12.9%) subtypes. The predominant subtype of the metastatic tumors in the cases in which the primary tumors showed the acinar-predominant subtype was the original acinar subtype (72.0%), followed by the solid (23.4%) and papillary (4.6%) subtypes. The predominant subtype of the metastatic lymph node tumors in the cases in which the primary tumors showed the solid-predominant

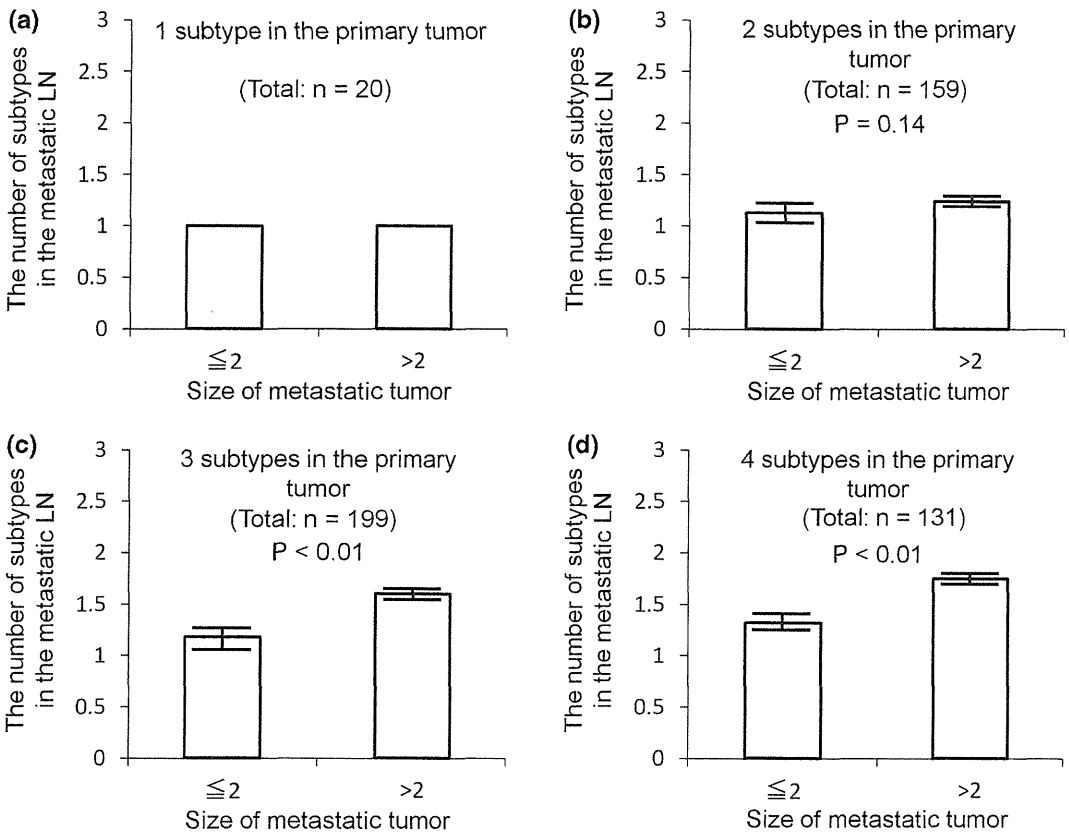

Figure 2 The number of component histologic subtypes in the metastatic lymph node tumors. (**a**) Comparison of the histologic subtypes in the group in which the primary tumor was composed of a single subtype. The mean number of histologic subtypes in both metastatic tumor size groups was 1.00. (**b**) Comparison in the group in which the primary tumor was composed of 2 subtypes (≤2 mm: 1.1, > 2 mm: 1.2: $P = 0.14$). (**c**) Comparison of the histologic subtypes in the group in which the primary tumor was composed 3 subtypes (≤2 mm: 1.2, > 2 mm: 1.6: $P < 0.01$). (**d**) Comparison of the histologic subtypes in the group in which the primary tumor was composed of 4 subtypes (≤2 mm: 1.3, > 2 mm: 1.8: $P < 0.01$).

Table 3 Comparison between the predominant histological subtypes in the primary tumors and the metastatic lymph node tumors

Predominant subtype		
Primary tumor	Metastatic LN tumor	(%)
Lepidic	Papillary	4 (50.0)
	Acinar	4 (50.0)
	Solid	0 (0.0)
Papillary	Papillary	92 (47.4)
	Acinar	25 (12.9)
	Solid	77 (39.7)
Acinar	Papillary	5 (4.6)
	Acinar	77 (72.0)
	Solid	25 (23.4)
Solid	Papillary	6 (3.0)
	Acinar	13 (6.5)
	Solid	181 (90.5)

subtype was the original solid subtype (90.5%), followed by the acinar (6.5%) and papillary (3.0%) subtypes. The solid-predominant subtype was identified at a high frequency in the metastatic lymph node tumors, even in cases in which the primary tumor showed other predominant subtypes.

Predominant histologic subtypes according to the sizes of the metastatic lymph node tumors

Next, we compared the predominant histologic subtype of the primary tumors and matched metastatic lymph node tumors in relation to the sizes of the metastatic lymph node tumors (Fig. 3).

1 Primary tumor showing the lepidic-predominant subtype; one case of the papillary-predominant and one of the acinar-predominant subtype were identified in metastatic

Table 4 The correlation between the metastatic lymph node predominant subtype and metastatic tumor size (≤2 mm and >2 mm) in a) papillary and b) acinar predominant primary tumor

a) in papillary predominant primary tumor			
	Predominant subtype		
Metastatic lymph node tumors	Papillary (%)	Non-Papillary (%)	*P*
Size			
≤2 mm	18 (35)	33 (65)	0.04
>2 mm	74 (52)	69 (48)	
b) in acinar predominant primary tumor			
	Predominant subtype		
Metastatic lymph node tumors	Acinar (%)	Non-Acinar (%)	*P*
Size			
≤2 mm	12 (55)	10 (45)	0.04
>2 mm	65 (76)	20 (24)	

lymph node tumors that were more than 5 mm in size (data not shown).

2 Primary tumor showing the papillary-predominant subtype; the most frequent subtype in the metastatic tumors that were ≤2 mm in size was the solid-predominant subtype (25/51, 49.0%), followed by the papillary subtype 35.3% (18/51). However, when the metastatic tumors grew to more than 5 mm in size, the most frequent subtype was the papillary subtype in 54.3% (44/81), followed by the solid subtype in 39.5% (32/81) (Fig. 3a).

3 Primary tumor showing the acinar-predominant subtype; the acinar- and solid-predominant subtypes were identified in 54.5% (12/22) and 36.4% (8/22) of metastatic lymph node tumors that were ≤ 2 mm in diameter, respectively. On the other hand, the acinar and solid subtypes were seen in 83.8% (31/37) and 10.8% (4/37), respectively, of metastatic lymph node that were more than 5 mm in diameter (Fig. 3b).

4 Primary tumors showing the solid-predominant subtype; the solid-predominant subtype was identified in 98.0% (48/49) of metastatic lymph node tumors that were ≤2 mm in diameter. The solid subtype was seen in 86.3% (88/102) of metastatic tumors that were more than 5 mm in diameter (Fig. 3c).

Comparison of the predominant histologic subtypes between metastatic lymph node tumors that were 2 cm or under and over 2 mm in diameter

Table 4 shows the correlation between the predominant histological subtype and the metastatic tumor size (≤2 mm vs. >2 mm) in cases in which the primary tumor showed the papillary- or acinar- predominant subtype.

When the predominant histologic subtype of the primary tumor was the papillary, 35% of metastatic tumors that were ≤2 mm in diameter showed the papillary-predominant subtype; however, the frequency of tumors showing the papillary-predominant subtype increased to 52% in the metastatic tumors that were >2 mm in diameter ($P = 0.04$).

In addition, when the predominant subtype of the primary tumor was the acinar subtype, 55% of metastatic tumors that were ≤2 mm in size showed the acinar-predominant subtype, with the frequency of this histologic subtype increasing to 76% in metastatic tumors that were >2 mm in diameter ($P = 0.04$).

DISCUSSION

In the present report, we found that the predominant histologic subtype of metastatic lymph node tumors that were 2 mm or less in size often differed from that of the primary tumor. Actually, even when the primary tumor showed the acinar- or papillary-predominant subtype, metastatic lymph node tumors that were small in size often showed a solid-predominant subtype. However, as the metastatic lymph node tumors increased in size, the original subtype began to appear. These findings suggest that the solid morphology could be the initiating feature of metastasis in the early phase of the lymph node metastatic process. Then, as the metastatic tumor cells engraft and grow in the lymph nodes, the tumor cell populations regain the original morphological features and diversity. This sequence implies that the histological and biological characteristics of tumor cells in the engraftment process are largely different from those of tumor cells in the development process of metastatic tumor formation.[14–16] This is the first study to evaluate the correlation between the sizes of the metastatic tumors and the histologic subtype and tumor cell diversity in cases of adenocarcinoma of the lung.

In a previous report about the histological characteristics of metastatic lymph node tumors, Sica *et al.* reported that the

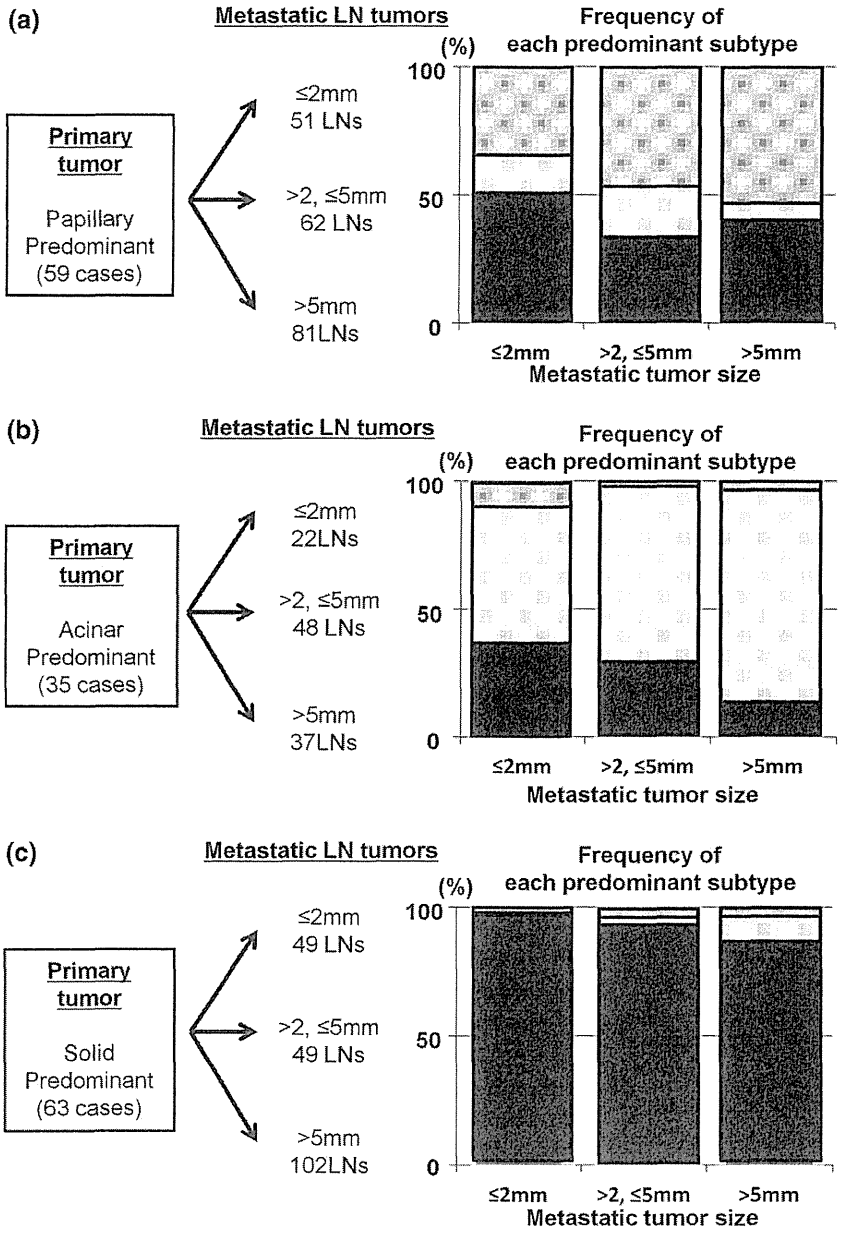

Figure 3 Comparison of the predominant histologic subtypes according to the sizes of the metastatic lymph node tumors. (**a**) Cases in which the primary tumor showed the papillary-predominant subtype. There were 51, 62 and 81 metastatic lymph node tumors that were ≤2 mm, > 2 mm but ≤5 mm and >5 mm in diameter respectively. Of the 51 metastatic tumors that were <2 mm in diameter, 25 (49%) showed the solid-predominant subtype and 18 (35%) showed the papillary-predominant subtype. Of the 81 metastatic tumors that were >5 mm in diameter, 32 (39%) showed the solid-predominant subtype and 44 (54%) showed the papillary-predominant subtype. (**b**) Cases in which the primary tumor showed the acinar-predominant subtype. There were 22, 48 and 37 metastatic lymph node tumors that were ≤2 mm, > 2 mm but ≤5 mm and >5 mm in diameter, respectively. Of the 22 metastatic tumors that were <2 mm in diameter, 12 (55%) showed the acinar-predominant subtype and 8 (36%) showed the solid-predominant subtype. Furthermore of the 37 metastatic tumors that were >5 mm in diameter, 31 (84%) showed the acinar-predominant subtype and 4 (11%) showed the solid-predominant subtype. (**c**) Cases in which the primary tumor showed the solid-predominant subtype. There were 49, 49 and 102 metastatic lymph node tumors that were ≤2 mm, > 2 mm but ≤5 mm and >5 mm in diameter, respectively. Of the 49 metastatic tumors that were <2 mm in diameter, 48 (90%) showed the solid-predominant subtype, and of the 102 metastatic tumors that were >5 mm in diameter, 87 (86%) showed the solid-predominant subtype. ▩, Papillary; □, Acinar; ▩, Solid.

predominant pattern of any primary tumor is more likely to be seen at the metastatic site, and even when the micropapillary and solid patterns are present only at a small percentage in the primary tumor, these patterns are often seen in the metastatic lymph node tumors.[17] While these findings were partly consistent with our current results, there was no reference to the correlation of the metastatic tumor size with the predominant histologic subtype in that study. Taking these observations and our current results into consideration, it may be speculated that the solid morphology may be an important feature reflecting metastasis-initiating cancer cells during the process of development of lymph node metastasis. Takuwa *et al.* reported that solid subtype in lung adenocarcinomas exhibits the invasive immunophenotype, including increased laminin-5 expression, which may, in part, be consistent with our hypothesis.[3]

In this study, the solid predominant subtype in the metastatic lymph node tumor is morphologically defined according to the primary tumor criterion. However, considering cancer stem/initiating cell theory, it is possible to think that biological features of the cancer cells showing 'solid' morphology in metastatic lymph node tumor are different from those of

primary lung tumor showing solid morphology. Further investigation will be needed whether these two morphologically similar tumors display different biological features.

Aokage, one of our colleagues, examined a large number of small intrapulmonary metastases in detail by applying the histological classification of primary adenocarcinoma of the lung to the metastatic tumors.[12] In this report, most intrapulmonary metastatic tumors arising from primary adenocarcinoma exhibited a lepidic-predominant histologic subtype in the early phase and the morphological diversity of the original tumor began to be reproduced as the tumor grew in size. This phenomenon was similar to our finding of recapitulation of the original morphological features as the metastatic tumors grew, but differed in that the major hisotologic subtype in the early phase of pulmonary metastatic tumors was the lepidic-predominant subtype, whereas in our study, it was the solid subtype. This difference suggests the possibility of the histological environment of the metastatic organs decisively affecting the tumor morphological features in the early phase of the metastatic process.

Recent studies have indicated the importance of transient EMT-MET switches in the metastatic process.[18–22] Chaffer *et al.* showed, using a bladder cell line, spontaneous shift from mesenchymal to epithelial characteristics and its association with increased metastatic ability in advanced malignancies.[23] Tsai *et al.* also reported, using a spontaneous squamous cell carcinoma in Twist 1 transgenic mouse model, that activation of Twist1 is sufficient to promote EMT of cancer cells and to disseminate the cells into the circulation, and also that turning off Twist1 is essential to allow reversal of EMT for dissemination of tumors to distant sites.[24] We also previously investigated the immunophenotypes of cancer cells in small metastatic lesions of the lung, and concluded that a dynamic phenotypic change that includes both EMT and MET occurs in the early phase of metastatic tumor formation.[25] Therefore, the solid histologic subtype is the important phenotype corresponding to the transitional phase of EMT-MET in the early stage of the metastatic process.

The cancer stem cell theory may explain the phenomenon of metastatic tumor cells reproducing the morphological diversity of the original tumor as the metastatic tumors grew in size.[26–30] According to the cancer stem cell concept, a single cell or a small number of cancer cells have the potential to reconstitute a primary tumor under favorable conditions and diversity of the tumor cell populations develops during tumor progression.

Successful formation of macroscopic metastatic tumors requires angiogenesis and several extrinsic factors in the microenvironment. Therefore, tumor microenvironment of micrometastases and macrometastasis would be obviously different. To examine the differences of cancer cell phenotype and the stromal reaction between in micrometastases and macrometastases gives us very important information to know the dynamism of tumor metastatic process. For further investigation, we are planning to examine the immunophenotypic differences between lymph node micrometastasis and macrometastasis.

In conclusion, we found a high percentage of cases showing the solid phenotype in the early phase of the lymph node metastatic process, and that the metastatic tumor cells tended to regain the original morphological features and diversity as the tumors grew in size. As a prognostic factor, the small lymph node metastasis is recently noted and prospective cohort surveys have been performed.[31–33] Clarification of the biological features of small lymph node metastases is important for the development of new strategies for early cancer detection and for the development of effective cancer treatment approaches.

REFERENCES

1 Travis WD, Brambilla E, Noguchi M *et al.* International association for the study of lung cancer/american thoracic society/european respiratory society international multidisciplinary classification of lung adenocarcinoma. *J Thorac Oncol* 2011; **6**: 244–85.
2 Lee HJ, Kim YT, Kang CH *et al.* Epidermal growth factor receptor mutation in lung adenocarcinomas: Relationship with CT characteristics and histologic subtypes. *Radiology* 2013; **268**: 254–64.
3 Takuwa T, Ishii G, Nagai K *et al.* Characteristic immunophenotype of solid subtype component in lung adenocarcinoma. *Ann Surg Oncol* 2012; **19**: 3943–52.
4 Russell PA, Wainer Z, Wright GM *et al.* Does lung adenocarcinoma subtype predict patient survival?: A clinicopathologic study based on the new International Association for the Study of Lung Cancer/American Thoracic Society/European Respiratory Society international multidisciplinary lung adenocarcinoma classification. *J Thorac Oncol* 2011; **6**: 1496–504.
5 Kim H, Yoo SB, Sun P *et al.* Alteration of the E-Cadherin/beta-catenin complex is an independent poor prognostic factor in lung adenocarcinoma. *Korean J Pathol* 2013; **47**: 44–51.
6 Zhang Y, Sun Y, Pan Y *et al.* Frequency of driver mutations in lung adenocarcinoma from female never-smokers varies with histologic subtypes and age at diagnosis. *Clin Cancer Res* 2012; **18**: 1947–53.
7 Gao D, Nolan DJ, Mellick AS *et al.* Endothelial progenitor cells control the angiogenic switch in mouse lung metastasis. *Science* 2008; **319**: 195–8.
8 Folkman J. Angiogenesis in cancer, vascular, rheumatoid and other disease. *Nat Med* 1995; **1**: 27–31.
9 Folkman J. Tumor angiogenesis: Therapeutic implications. *N Engl J Med* 1971; **285**: 1182–6.
10 Ksiazkiewicz M, Markiewicz A, Zaczek AJ. Epithelial-mesenchymal transition: A hallmark in metastasis formation linking circulating tumor cells and cancer stem cells. *Pathobiology* 2012; **79**: 195–208.
11 Brabletz T, Jung A, Reu S *et al.* Variable beta-catenin expression in colorectal cancers indicates tumor progression driven by the tumor environment. *Proc Natl Acad Sci USA* 2001; **98**: 10356–61.
12 Aokage K, Ishii G, Yoshida J *et al.* Histological progression of small intrapulmonary metastatic tumor from primary lung adenocarcinoma. *Pathol Int* 2010; **60**: 765–73.

13 International Union against Cancer, Sobin LH, Gospodrowicz MK, Wittekind CH, eds. *TNM Classification of Malignant Tumours*, 7th edn. New York: Wiley-Liss, 2009.
14 Yeung TM, Buskens C, Wang LM *et al.* Myofibroblast activation in colorectal cancer lymph node metastases. *Br J Cancer* 2013; **108**: 2106–15.
15 Yanagita S, Natsugoe S, Uenosono Y *et al.* Sentinel node micrometastases have high proliferative potential in gastric cancer. *J Surg Res* 2008; **145**: 238–43.
16 Yokoyama H, Nakanishi H, Kodera Y *et al.* Biological significance of isolated tumor cells and micrometastasis in lymph nodes evaluated using a green fluorescent protein-tagged human gastric cancer cell line. *Clin Cancer Res* 2006; **12**: 361–8.
17 Sica G, Yoshizawa A, Sima CS *et al.* A grading system of lung adenocarcinomas based on histologic pattern is predictive of disease recurrence in stage I tumors. *Am J Surg Pathol* 2010; **34**: 1155–62.
18 Chao YL, Shepard CR, Wells A. Breast carcinoma cells re-express E-cadherin during mesenchymal to epithelial reverting transition. *Mol Cancer* 2010; **9**: 179.
19 Klymkowsky MW, Savagner P. Epithelial-mesenchymal transition: A cancer researcher's conceptual friend and foe. *Am J Pathol* 2009; **174**: 1588–93.
20 Hudson LG, Zeineldin R, Stack MS. Phenotypic plasticity of neoplastic ovarian epithelium: Unique cadherin profiles in tumor progression. *Clin Exp Metastasis* 2008; **25**: 643–55.
21 Hugo H, Ackland ML, Blick T *et al.* Epithelial—mesenchymal and mesenchymal—epithelial transitions in carcinoma progression. *J Cell Physiol* 2007; **213**: 374–83.
22 Chaffer CL, Thompson EW, Williams ED. Mesenchymal to epithelial transition in development and disease. *Cells Tissues Organs* 2007; **185**: 7–19.
23 Chaffer CL, Brennan JP, Slavin JL *et al.* Mesenchymal-to-epithelial transition facilitates bladder cancer metastasis: Role of fibroblast growth factor receptor-2. *Cancer Res* 2006; **66**: 11271–8.
24 Tsai JH, Donaher JL, Murphy DA *et al.* Spatiotemporal regulation of epithelial-mesenchymal transition is essential for squamous cell carcinoma metastasis. *Cancer Cell* 2012; **22**: 725–36.
25 Aokage K, Ishii G, Ohtaki Y *et al.* Dynamic molecular changes associated with epithelial-mesenchymal transition and subsequent mesenchymal-epithelial transition in the early phase of metastatic tumor formation. *Int J Cancer* 2011; **128**: 1585–95.
26 Visvader JE, Lindeman GJ. Cancer stem cells in solid tumours: Accumulating evidence and unresolved questions. *Nat Rev Cancer* 2008; **8**: 755–68.
27 Kakarala M, Wicha MS. Implications of the cancer stem-cell hypothesis for breast cancer prevention and therapy. *J Clin Oncol* 2008; **26**: 2813–20.
28 Morel AP, Lievre M, Thomas C *et al.* Generation of breast cancer stem cells through epithelial-mesenchymal transition. *PLoS ONE* 2008; **3**: e2888.
29 Mani SA, Guo W, Liao MJ *et al.* The epithelial-mesenchymal transition generates cells with properties of stem cells. *Cell* 2008; **133**: 704–15.
30 Hermann PC, Huber SL, Herrler T *et al.* Distinct populations of cancer stem cells determine tumor growth and metastatic activity in human pancreatic cancer. *Cell Stem Cell* 2007; **1**: 313–23.
31 Rusch VW, Hawes D, Decker PA *et al.* Occult metastases in lymph nodes predict survival in resectable non-small-cell lung cancer: Report of the ACOSOG Z0040 trial. *J Clin Oncol* 2011; **29**: 4313–9.
32 de Boer M, van Deurzen CH, van Dijck JA *et al.* Micrometastases or isolated tumor cells and the outcome of breast cancer. *N Engl J Med* 2009; **361**: 653–63.
33 Yasumoto K, Osaki T, Watanabe Y *et al.* Prognostic value of cytokeratin-positive cells in the bone marrow and lymph nodes of patients with resected nonsmall cell lung cancer: A multicenter prospective study. *Ann Thorac Surg* 2003; **76**: 194–201.

Ann Surg Oncol (2014) 21:3608–3615
DOI 10.1245/s10434-014-3762-y

Annals of
SURGICAL ONCOLOGY
OFFICIAL JOURNAL OF THE SOCIETY OF SURGICAL ONCOLOGY

ORIGINAL ARTICLE – COLORECTAL CANCER

Long-term Outcomes after Intersphincteric Resection for Low-Lying Rectal Cancer

Norio Saito, MD, PhD[1], Masaaki Ito, MD, PhD[1], Akihiro Kobayashi, MD, PhD[1], Yusuke Nishizawa, MD, PhD[1], Motohiro Kojima, MD, PhD[2], Yuji Nishizawa, MD, PhD[1], and Masanori Sugito, MD, PhD[1]

[1]Department of Colorectal Surgery, National Cancer Center Hospital East, Chiba, Japan; [2]Pathology Division, Research Center for Innovative Oncology, National Cancer Center Hospital East, Chiba, Japan

ABSTRACT

Background. As an anus-preserving surgery for very low rectal cancer, intersphincteric resection (ISR), has advanced markedly over the last 20 years. We investigated long-term oncologic, functional, and quality of life (QOL) outcomes after ISR with or without partial external sphincter resection (PESR).

Methods. A series of 199 patients underwent curative ISR with or without PESR between 2000 and 2008, with 49 receiving preoperative chemoradiotherapy (CRT group) and 150 undergoing surgery first (surgery group). Overall survival (OS), disease-free survival (DFS), and local relapse-free survival (LFS) rates were calculated using Kaplan–Meier methods. Functional outcomes were assessed using the Wexner incontinence score. QOL was investigated using the Short-Form 36 questionnaire (SF-36) and modified fecal incontinence quality of life (mFIQL) scale.

Results. After a median follow-up of 78 months (range 12–164 months), estimated 7-year OS, DFS, and LFS rates were 78, 67, and 80 %, respectively. LFS was better in the CRT group than in the surgery group ($p = 0.045$). Patients with PESR or positive circumferential resection margins showed significantly worse survival. The median Wexner incontinence score at >5 years was 8 in the surgery group and 10 in the CRT group ($p = 0.01$). QOL was improved in all physical and mental subscales of the SF-36 at >5 years. Although the mFIQL showed a relatively good score in all groups at >5 years, a significant difference existed between the CRT and surgery groups ($p = 0.008$).

Conclusions. With long-term follow-up, oncologic, functional, and QOL results after ISR appear acceptable, although CRT is associated with disturbance.

First Received: 29 November 2013;
Published Online: 13 June 2014

N. Saito, MD, PhD
e-mail: norsaito@east.ncc.go.jp

The main therapy for rectal cancer is curative surgical resection. Surgery for rectal cancer has three main objectives: cure of cancer, preservation of anal function, and maintenance of quality of life (QOL). Total excision of the mesorectum as developed by Heald and Ryall[1] has led to improved local control and survival.

Next to radical resection of the tumor, anus-preserving surgery is one of the major goals for lower rectal cancer. Lower rectal cancer located within 5 cm from the anal verge has traditionally been treated using abdominoperineal resection. However, anus-preserving operations for very low rectal cancer have advanced over the last 20 years with the new procedure of intersphincteric resection (ISR). Some authors have proposed ISR to increase the chance of sphincter-saving resection for selected low rectal tumors.[2–14] Combined with neoadjuvant chemoradiotherapy (CRT), ISR has been used to extend the opportunity for sphincter preservation. Although ideal candidates for ISR are limited to patients with the lower edge of T1 and T2 tumors lying >1 cm from the intersphincteric groove, we have extended the indications for ISR to T3 and part of T4 disease by using the technique combined with partial external sphincter resection (PESR) or preoperative CRT.

The aim of this study was to assess long-term oncologic, functional, and QOL outcomes after ISR with or without PESR.

METHODS

Patients

In total, 1,033 consecutive patients with rectal cancer received curative surgical treatment at our institute from

2000 to 2008. Of these, 93 % underwent anus-preserving surgery. Participants in the present study comprised 199 patients who underwent curative ISR with or without PESR for low rectal cancers after being prospectively enrolled.

Informed consent was obtained from each patient, and all study protocols were approved by the hospital ethics committee. ISR with or without PESR was indicated for tumors located within 5 cm from the anal verge. The exact level of the lower edge of the tumor from the anal verge was assessed and measured by digital examination and endoscopy. An exception to selection of ISR with or without PESR was made if the patient showed definitive invasion of the external sphincter or levator ani muscle. Patients with significant clinical fecal incontinence (more than once per week) were also excluded. All patients underwent preoperative imaging of the chest, abdomen, and pelvis, usually with computed tomography and either magnetic resonance imaging or endorectal ultrasonography.

Operative Techniques

The surgical technique included both abdominal and transanal approaches. In the abdominal approach, total mesorectal excision and pelvic lateral node dissection with or without autonomic nerve preservation were performed, although lateral node dissection is not the standard of care outside Japan. The rectum was mobilized as low as possible to the pelvic floor to facilitate the transanal approach. The surgical anal canal was then divided circumferentially from the puborectal muscle and external sphincter. If the tumor adhered to the puborectal muscle and/or external sphincter, those structures were partially resected to obtain adequate safety margins. Fatty tissue of the ischiorectal fossa was thus sometimes visualized. This procedure of PESR has been reported previously.[6,12] Defects in the external sphincter were repaired as much as possible by using manual transanal suturing. Most patients underwent end-to-end coloanal anastomosis. Finally, a diverting stoma was established and closed 3 months postoperatively or after completion of adjuvant chemotherapy.

ISR was classified into three types: total ISR, subtotal ISR, and partial ISR. Total ISR involved complete excision of the internal sphincter for tumors spreading to or beyond the dentate line. The distal cut-end line was at the intersphincteric groove. In partial ISR, the distal cut-end line was just on or slightly above the dentate line, and the distal cut-end line was between the dentate line and intersphincteric groove in subtotal ISR.

Adjuvant Therapy

Preoperative CRT was performed in 49 patients with clinical T3 tumors who agreed to preoperative adjuvant therapy. Other patients underwent surgery without CRT, because preoperative CRT for resectable rectal cancer is still not standard in Japan. Forty-nine patients received 45 Gy of radiotherapy administered with continuous infusion of 5-fluorouracil (250 mg/m^2 day) during the 5-week period preceding surgery. Ninety-five patients with stage IIA, stage IIB, or III (pTMN pathologic classification) received postoperative chemotherapy with 5-fluorouracil and folinic acid or tegafur uracil for 6 months.[15]

Follow-up

Patients were followed up by using a standardized protocol (including clinical examination with digital palpation; computed tomography of the chest, abdomen, and pelvis; and measurement of tumor marker levels) every 4 months for the first 2 years, then every 6 months for 3 years, then annually thereafter. Total colonoscopy was performed at 2 and 5 years after surgery.

Functional and QOL Assessment

Patients who remained alive without recurrence after follow-up for $\geq$60 months were eligible for the functional study. Exclusion criteria were death, pelvic recurrence, definitive stoma for anastomotic trouble or poor function, and psychiatric disorders.

Functional assessment was performed every year after stoma closure by using our functional questionnaire. This questionnaire asked about stool frequency (per 24 h), feces and flatus discrimination, urgency (ability to defer stool evacuation for >15 min), fragmentation ($\geq$2 evacuations in 1 h), soiling during the day and night, use of pads, use of medications, alimentary restriction, and lifestyle alteration. Questionnaires were regularly sent to patients. Incontinence was assessed by using the Wexner score, where 0 represents perfect continence and 20 indicates major incontinence. Functional outcomes were considered "poor" for Wexner scores >10, whereas scores $\leq$10 were considered "good".[16,17]

The Japanese version of the Short-Form 36 questionnaire (SF-36) was applied as a nonspecific, general evaluation of QOL.[18,19] The SF-36 consists of eight multi item scales: physical function, role limitations-physical, bodily pain, general health, vitality, social function, role limitation-emotional, and mental health. On the basis of these subscales, component summary scores can be calculated to provide a global measure of physical function (physical component summary; PCS) and mental function (mental component summary; MCS), respectively. Scale scores ranged from 0 to 100, with higher scores indicating better health status.

TABLE 1 Characteristics of patients undergoing ISR with or without PESR

Variable	Total ($n = 199$)	CRT group ($n = 49$)	Surgery group ($n = 150$)	p value
Age (years) median (range)	59 (27–80)	56 (27–77)	60 (32–80)	0.048
Male/female	144/55	38/11	106/44	0.875
AV mean (cm)	3.8	3.5 (1.5–5)	4.0 (0.6–7)	0.011
Tumor stage (clinical)				0.217
cT1	6	0	6	
cT2	38	9	29	
cT3	136	38	98	
cT4 (prostate, vagina, etc.)	19	2	17	
Operation type (ISR)				
Total	55	23	32	
Subtotal	80	17	63	
Partial	64	9	55	
ISR with PESR	41(20.6 %)	(9)	(32)	
Positive circumferential resection margin (CRM $\leq$1 mm)[a]	39 (19.6)	6 (12.2)	33 (22.0)	0.135
Lateral lymph node metastasis	24 (12.1)	7 (14.3)	17 (11.3)	0.582
Pathologic stage (pTNM)				
0	9 (4.5)	8 (16.3)	0 (0.0)	
I	69 (34.7)	15 (30.6)	55 (36.7)	
IIA	44 (22.1)	8 (16.3)	36 (24.0)	
IIB	2 (1.0)	1 (2.0)	1 (0.7)	
IIIA	10 (5.0)	1 (2.0)	9 (6.0)	
IIIB	27 (13.6)	8 (16.3)	19 (12.7)	
IIIC	38 (19.1)	8 (16.3)	30 (20.0)	
Anastomotic dehiscence	20 (10.1)	8 (16.3)	12 (8.0)	0.083
Definitive stoma	20 (10.1)	11 (22.4)	9 (6.0)	0.002
Not closed (diverting stoma)	12 (6.0)	5 (10.2)	7 (4.7)	0.143
Anastomotic trouble	5	3	2	
Recurrence, others	7	2	5	
Reestablished	8 (4.0)	6 (12.2)	2 (1.3)	0.003
Poor bowel function	4	3	1	
Recurrence (APR)	4	3	1	

Data are n (%) unless otherwise noted

CRT preoperative chemoradiotherapy (45 Gy; 5-fluorouracil), *ISR* intersphincteric resection, *PESR* partial external sphincter resection, *APR* abdominoperineal resection

[a] Positive pathologic margin: 0

The Japanese version of the modified fecal incontinence quality of life (mFIQL) questionnaire was used as a specific and sensitive QOL questionnaire.[20] This questionnaire explores 14 items, with each response to a specific item assigned a value from 1 to 4 and summarized in a score. Scale scores ranged from 0 to 100, with higher scores indicating worse QOL.

Statistical Analysis

Patients were divided into groups as follows: ISR without CRT (surgery group) and ISR with CRT (CRT group); ISR only (ISR group) and ISR with PESR (PESR group); and positive surgical circumferential resection margin (CRM) and negative surgical CRM groups. Positive surgical CRM was defined as tumor $\leq$1 mm from the CRM.[21–23]

Overall survival (OS), disease-free survival (DFS), and local relapse-free survival (LFS) rates were calculated by using Kaplan–Meier methods. Differences between curves were evaluated with the log-rank test. Univariate and multivariate analyses were performed to assess the impact of clinical, surgical, and treatment variables on functional

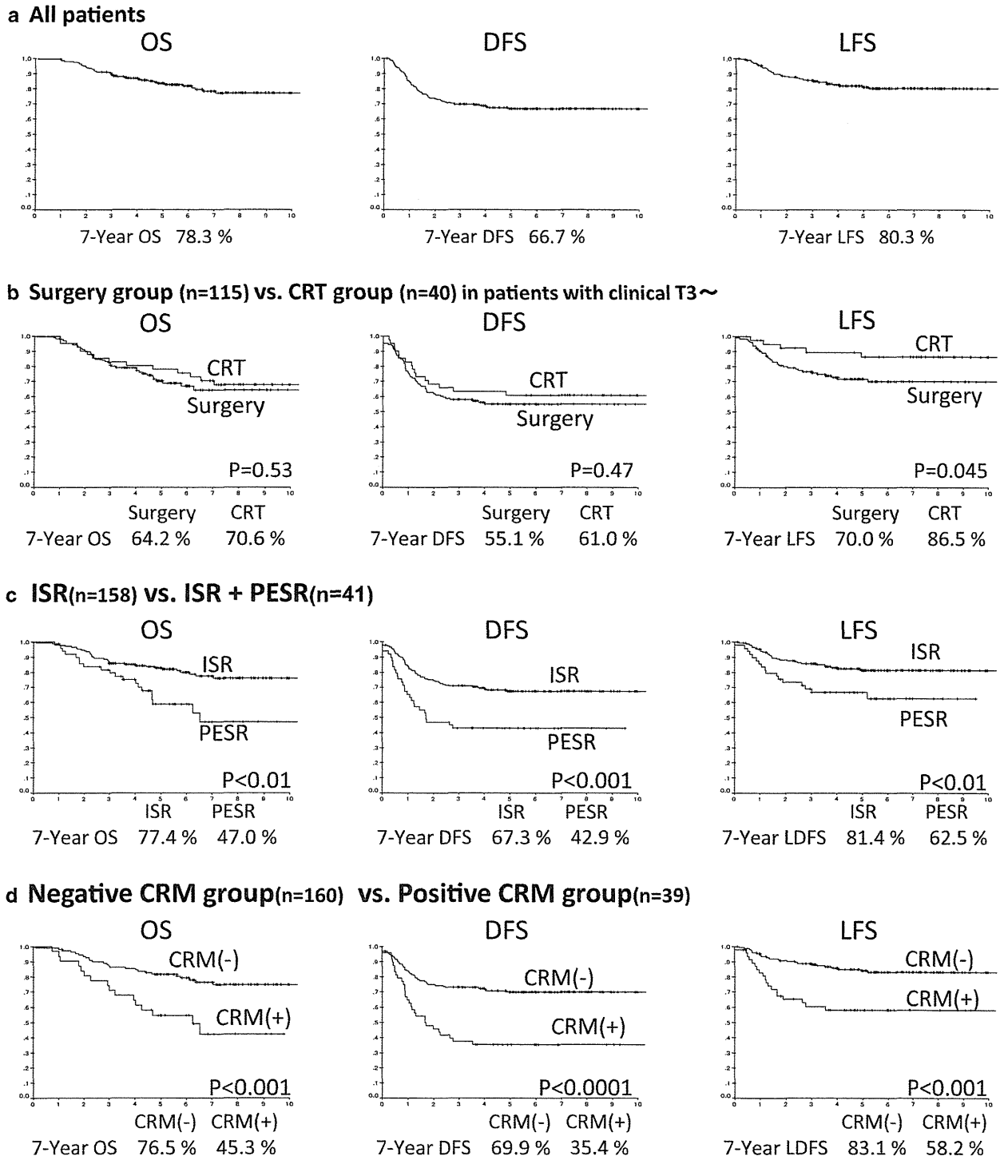

FIG. 1 Kaplan-Meier survival after ISR ± PESR. **a** All patients. **b** Surgery group ($n = 115$) versus CRT group ($n = 40$) in patients with clinical T3～. **c** ISR (n = 158) versus ISR + PESR ($n = 41$). **d** Negative CRM group ($n = 160$) versus positive CRM group ($n = 39$)

TABLE 2 Functional results at 2 or >5 years after stoma closure

Variable	2 Years ($n = 116$)	>5 Years ($n = 104$)
Stool frequency per 24 h (mean ± SD)	4.7 ± 4.6	4 ± 3.5
Fecal urgency (% of n)	30	32
Feces/flatus discrimination (% of n)	16	18
Stool fragmentation (% of n)	43	51
Difficult evacuation (% of n)	17	25
Daytime soiling (% of n)	35	30
Nighttime soiling (% of n)	30	26
Incontinence to gas (% of n)	56	55
Pad wearing (% of n)	50	55
Lifestyle alteration (% of n)	34	21

outcome. Data on postoperative functions and QOL are given as median and range. Differences between groups were tested by using the unpaired t test and the Chi square test or Fischer's exact test, as appropriate. Statistical evaluation was performed with SPSS for Windows version 20.0 software (SPSS, Chicago, IL). Values of $p < 0.05$ were considered statistically significant.

RESULTS

Details of patient characteristics in the CRT and surgery groups are listed in Table 1. Overall, 150 patients underwent curative ISR without preoperative CRT. PESR was performed in 41 patients (20.6 %). Of these, 29 had not undergone preoperative CRT. The CRT and surgery groups were comparable with respect to demographics and treatment characteristics except for tumor location. The median distance between the lower edge of the tumor and anal verge was 3.5 cm (range 1–5.5 cm) in the CRT group and 4.0 cm (range 0.6–6 cm) in the surgery group. The rate of pathologic lateral lymph node metastasis was 12.1 % in all patients.

Oncologic Results

After a median follow-up of 6.5 years (range 12–164 months), pulmonary metastasis, local recurrence with or without distant metastasis, liver metastasis, and combined recurrence occurred in 28 patients (14.1 %), 27 patients (13.6 %), 15 patients (7.5 %), and 9 patients (4.5 %), respectively. Nine patients with only local recurrence received salvage surgery (abdominoperineal resection, n = 4; tumor resection, $n = 5$). Seven-year OS, DFS, and LFS rates in all ISR patients were 78.3, 66.7, and 80.3 %, respectively (Fig. 1a). No significant differences in OS and DFS were identified between the surgery and CRT groups. The CRT group showed a tendency to decrease local recurrences ($p = 0.045$; Fig. 1b). The PESR group showed significantly worse survival than the ISR group, with 7-year OS rates of 77.4 % for the ISR group and 47.0 % for the PESR group ($p < 0.01$) and 7-year DFS rates of 67.3 % for the ISR group and 42.9 % for the PESR group ($p < 0.01$; Fig. 1c). Survival rates in the positive and negative CRM groups are shown in Fig. 1d. The positive CRM group displayed significantly worse OS, DFS, and LFS than the negative CRM group, with 7-year OS rates of 45.3 % for the positive CRM group and 76.5 % for the negative CRM group ($p < 0.001$). Seven-year DFS rates were 35.4 % for the positive CRM group and 69.9 % for the negative CRM group ($p < 0.0001$). Seven-year LFS rates were 58.2 % for the positive CRM group and 83.1 % for the negative CRM group ($p < 0.001$).

Functional Results

Of the 199 patients with curative ISR including PESR, 131 were candidates for evaluation of function and QOL at >5 years, and 104 patients (79.4 %) who responded to the questionnaire were assessed for continence function and QOL.

Mean stool frequency per 24 h was 4.0 ± 3.7. Approximately 50 % of patients had stool fragmentation and incontinence to gas, 30 % still experienced soiling during the day and at nighttime, and a quarter suffered from difficulties in evacuation (Table 2).

The median Wexner score was 8.5 (range 0–20) in all patients at >5 years after stoma closure. The CRT group showed significantly higher scores (median 10; range 4–20) than the surgery group (median 8; range 0–20; $p = 0.01$), although 70 % of patients showed good continence status (Wexner score 0–10; Fig. 2a). Univariate and multivariate analyses of functional outcomes are shown in Table 3. Significant effects on functional outcome were seen for sex and neoadjuvant treatment, although no effects were shown for age, tumor characteristics such as category or distance, or operative type. Female patients and the surgery group showed better continence function (female vs. male, $p = 0.01$; surgery vs. CRT, $p = 0.02$). Furthermore, similar findings were shown in multivariate analyses (Table 3).

QOL Results

QOL was improved in all physical and mental subscales (PCS and MCS) of the SF-36 at >5 years after ISR. No difference in PCS score was seen between the CRT and surgery groups (Fig. 2b-i). The CRT group showed worse MCS scores than the surgery group ($p = 0.02$). In addition, the mFIQL score differed significantly between the CRT and surgery groups (48 vs. 23; $p = 0.008$), although the

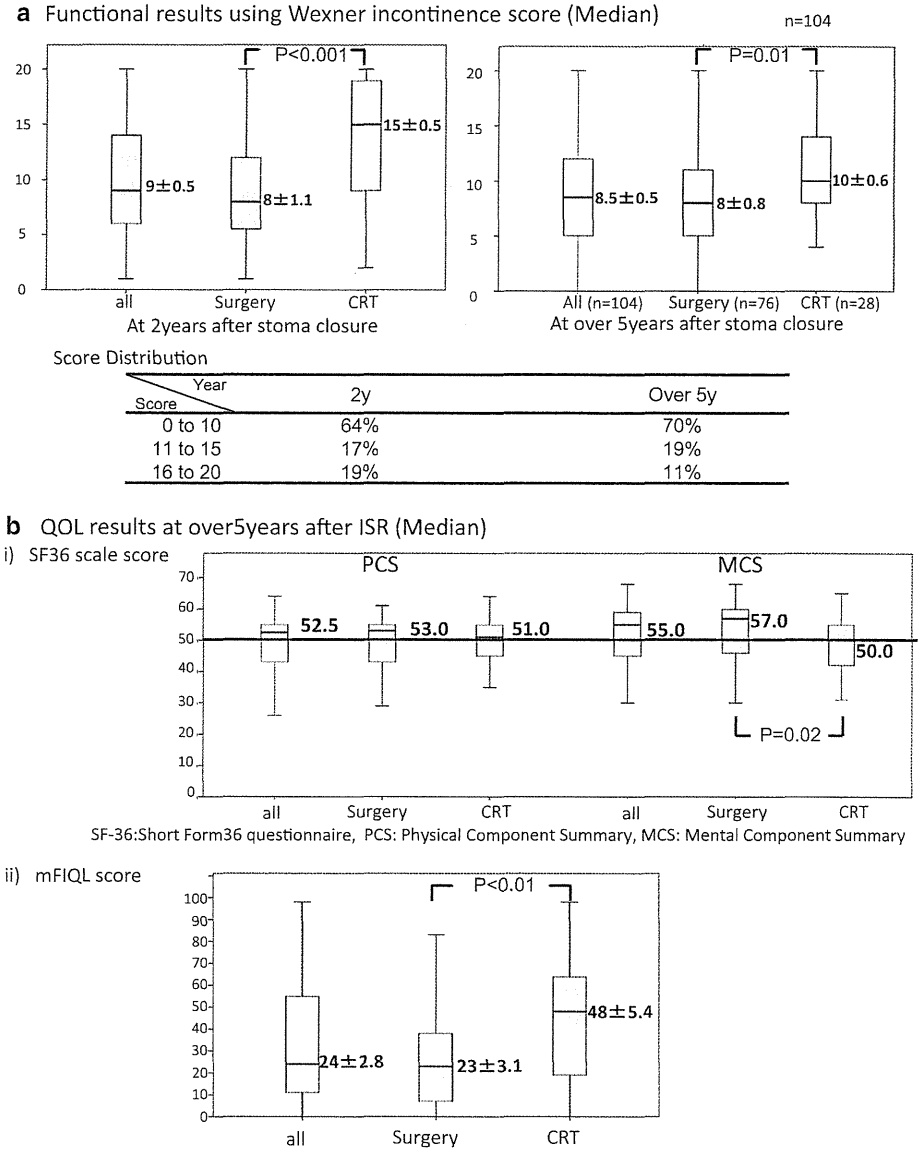

FIG. 2 Functional and QOL results. **a** Functional results according to the Wexner incontinence score (median). **b** QOL results at >5 years after ISR (median). *(i)* SF-36 scale score; *(ii)* mFIQL score

mFIQL showed relatively good status in all patients at >5 years (Fig. 2b-ii).

DISCUSSION

This study was designed to investigate long-term oncologic, functional, and QOL outcomes after ISR under extended indications. Many reports have described acceptable oncologic and functional results of ISR with mid-term observations, but few have examined long-term functional and QOL outcomes after ISR.

Our data with a median follow-up of 78 months showing a 7-year OS rate of 76.6 % were comparable to results from other studies. According to a systematic review of outcomes after ISR, the mean 5-year OS rate was 86.3 % (range 62–97 %), the DFS rate was 78.6 % (range 69–87 %), and the mean local recurrence rate was 6.7 % (range 0–23 %) at a median follow-up of 56 months.[24] In patients with clinical T3 or T4 tumors, neoadjuvant CRT tended to decrease local recurrences after ISR, although no differences in OS or DFS were seen. Conversely, significant differences in OS, DFS, and LFS were identified between ISR and PESR groups. The PESR group showed worse survival outcomes than the ISR group. Candidates for PESR should be selected with great care, and neoadjuvant therapy should be administered, because these patients have extended T3–4 tumors, and surgery alone offers limited efficacy for achieving local control. In the

TABLE 3 Factors influencing functional outcome according to the Wexner score

Univariate analysis	*n*	Median Wexner score	*p* Value
Preoperative radiotherapy			0.01
Yes	27	10	
No	77	8	
Sex			0.019
Male	76	9	
Female	28	6.5	
Age			0.707
≦65 years	78	8	
>65 years	26	9	
Type of surgery			0.654
Total ISR	26	9	
Subtotal ISR and partial ISR	78	8	
PESR			0.953
PESR	16	9	
ISR	88	8.5	
Tumor category			0.401
T1–T2	29	8	
T3–T4	75	9	
Distance from anal verge			0.649
<4 cm	42	9	
≧4 cm	62	8	

Multivariate analysis (multiple linear regression model)

	Coefficient (β)	SE	95 % CI	*p* Value
Intercept	16.087	2.161		
Preoperative CRT	−2.553	1.042	−4.620 to −0.486	0.016
Sex	−2.076	1.030	−4.119 to −0.033	0.046

PESR group, patients showed a higher positive CRM rate (36.7 %). Quirke et al.[22] reported CRM involvement as a key factor in rectal cancer treatment. The positive CRM group in this study showed worse prognosis. Additional therapy (radiation and abdominoperineal resection) should be considered in the positive CRM group, although no patient in this study received such treatment.

The next question to be answered concerns long-term functional and QOL outcomes. This operation involves side effects of internal sphincter resection or PESR. In our study, 70 % of patients showed good continence (Wexner score ≤10) at >5 years, although fragmentation, gas incontinence, and soiling were still experienced. The operative type of ISR did not matter for the long-term functional outcomes, as shown in other reports.[7,17] However, significant differences in continence were evident between male and female patients and between CRT and surgery groups. In particular, preoperative CRT was a strong predictor of incontinence in both univariate and multivariate analyses. Similar results have been reported in our own and other previous reports.[7,25] However, Denost et al.[17] reported that the risk of fecal incontinence after ISR depended on tumor level and height of the anastomosis. Various factors including cultural and social factors may exert influences on anal function. In our experience, postoperative anal function was decreased when CRT was very effective in patients undergoing ISR. One reason for worsened anal function may be marked neural degeneration caused by preoperative CRT.[26] However, we cannot definitively answer why postoperative anal function was better in female patients.

According to a QOL study by Sprangers et al.[27] patients with a permanent stoma experienced greater restrictions to level of social function than patients with ultralow resection. Conversely, Renner et al.[28] reported no differences in SF-36 scores between patients with coloanal anastomosis and those with anterior resection. In the present study, patients after ISR with or without PESR showed PCS and MCS at >5 years equal to or better than those preoperatively. Our results show that general QOL is acceptable in patients treated by ISR. The most popular scale used for measuring patient perception of fecal incontinence is the fecal incontinence QOL scale.[29] We demonstrated that mFIQL offers satisfactory psychometric reliability and validity for assessing the psychosocial dimension of QOL among patients after ISR.[20] The CRT group showed significantly worse mFIQL scores than the surgery group after long-term follow-up. This suggests that more functional problems might be associated with fecal incontinence in the CRT group. Therefore, new neoadjuvant therapies without radiation as an alternative to CRT may be necessary for obtaining better function and QOL, although CRT offers better local control. These results came from our single-center study, and comparative series involving multiple centers would be more useful for assessing function and QOL.

In conclusion, ISR with negative CRM represents a feasible surgical option in terms of oncologic outcomes for patients with very low rectal cancer at long-term follow-up. Long-term results for postoperative anal function and QOL are also acceptable in the majority of patients, although CRT is associated with disturbance.

ACKNOWLEDGMENT This study was supported in part by a Grant-in-Aid from the National Cancer Center (NCC) Research and Development Fund (23-A-26) in Japan.

CONFLICT OF INTEREST The authors declare no conflicts of interest.

REFERENCES

1. Heald RJ, Ryall RD. Recurrence and survival after total mesorectal excision for rectal cancer. *Lancet.* 1986;1:1479–82.
2. Schiessel R, Karner-Hanusch J, Herbst F, et al. Intersphincteric resection for low rectal tumours. *Br J Surg.* 1994;81:1376–8.
3. Bannon JP, Marks GJ, Mohiuddin M, et al. Radical and local excisional methods of sphincter-sparing surgery after high-dose radiation for cancer of the distal 3 cm of the rectum. *Ann Surg Oncol.* 1995;2:221–7.
4. Braun J, Treutner KH, Winkeltau G, et al. Results of intersphincteric resection of the rectum with direct coloanal anastomosis for rectal carcinoma. *Am J Surg.* 1992;163:407–12.
5. Rullier E, Laurent C, Bretagnol F, et al. Sphincter-saving resection for all rectal carcinomas: the end of the 2-cm distal rule. *Ann Surg.* 2005;241:465–9.
6. Saito N, Moriya Y, Shirouzu K, et al. Intersphincteric resection in patients with very low rectal cancer: a review of the Japanese experience. *Dis Colon Rectum.* 2006;49(10 Suppl.):S13–22.
7. Chamlou R, Parc Y, Simon T, et al. Long-term results of intersphincteric resection for low rectal cancer. *Ann Surg.* 2007;246:916–21.
8. Akasu T, Takawa M, Yamamoto S, et al. Intersphincteric resection for very low rectal adenocarcinoma: univariate and multivariate analyses of risk factors for recurrence. *Ann Surg Oncol.* 2008;15:2668–76.
9. Schiessel R, Novi G, Holzer B, et al. Technique and long-term results of intersphincteric resection for low rectal cancer. *Dis Colon Rectum.* 2005;48:1858–65.
10. Hohenberger W, Merkel S, Matzel K, et al. The influence of abdomino-peranal (intersphincteric) resection of lower third rectal carcinoma on the rates of sphincter preservation and locoregional recurrence. *Colorectal Dis.* 2006;8:23–33.
11. Yamada K, Ogata S, Saiki Y, et al. Long-term results of intersphincteric resection for low rectal cancer. *Dis Colon Rectum.* 2009;52:1065–71.
12. Saito N, Sugito M, Ito M, et al. Oncologic outcome of intersphincteric resection for very low rectal cancer. *World J Surg.* 2009;33:1750–6.
13. Weiser MR, Quah HM, Shia J, et al. Sphincter preservation in low rectal cancer is facilitated by preoperative chemoradiation and intersphincteric dissection. *Ann Surg.* 2009;249:236–42.
14. Krand O, Yalti T, Tellioglu G, et al. Use of smooth muscle plasty after intersphincteric rectal resection to replace a partially resected internal anal sphincter: long-term follow-up. *Dis Colon Rectum.* 2009;52:1895–901.
15. Jorge JM, Wexner SD. Etiology and management of fecal incontinence. *Dis Colon Rectum.* 1993;36:77–97.
16. Sobin LH, Wittekind Ch. International Union Against Cancer TMN classification of malignant tumours, 6th ed. New York: Wiley-Liss; 2002.
17. Denost Q, Laurent C, Capdepont MCRA, et al. Risk factors for fecal incontinence after intersphincteric resection for rectal cancer. *Dis Colon Rectum.* 2011;54:963–8.
18. Hashimoto H, Green J, Iwao Y, et al. Reliability, validity, and responsiveness of the Japanese version of the Inflammatory Bowel Disease Questionnaire. *J Gastroenterol.* 2003;38:1138–43.
19. Fukuhara S, Bito S, Green J, et al. Translation, adaptation, and validation of the SF-36 Health Survey for use in Japan. *J Clin Epidemiol.* 1998;51:1037–44.
20. Hashimoto H, Shiokawa H, Funahashi K, et al. Development and validation of a modified fecal incontinence quality of life scale for Japanese patients after intersphincteric resection for very low rectal cancer. *J Gastroenterol.* 2010;45:928–35.
21. Nagtegaal ID, Quirke P. What is the role for the circumferential margin in the modern treatment of rectal cancer? *J Clin Oncol.* 2008;26:303–12.
22. Quirke P, Steele R, Monson J, et al. Effect of the plane of surgery achieved on local recurrence in patients with operable rectal cancer: a prospective study using data from the MRC CR07 and NCIC-CTG CO16 randomised clinical trial. *Lancet.* 2009;373:821–28.
23. Taylor FGM, Quirke P, Heald RJ, et al. One millimetre is the safe cut-off for magnetic resonance imaging prediction of surgical margin status in rectal cancer. *Br J Surg.* 2011;98:872–9.
24. Martin ST, Heneghan HM, Winter DC. Systematic review of outcomes after intersphincteric resection for low rectal cancer. *Br J Surg.* 2012;99:603–12.
25. Ito M, Saito N, Sugito M, et al. Analysis of clinical factors associated with anal function after intersphincteric resection for very low rectal cancer. *Dis Colon Rectum.* 2009;52:64–70.
26. Nishizawa Y, Fujii S, Saito N, et al. The association between anal function and neural degeneration after preoperative chemoradiotherapy followed by intersphincteric resection. *Dis Colon Rectum.* 2011;54:1423–9.
27. Sprangers MA, Taal BG, Aaronson NK, et al. Quality of life in colorectal cancer. Stoma vs. nonstoma patients. *Dis Colon Rectum.* 1995;38:361–9.
28. Renner K, Rosen HR, Novi G, et al. Quality of life after surgery for rectal cancer: do we still need a permanent colostomy? *Dis Colon Rectum.* 1999;42:1160–7.
29. Rockwood TH, Church JM, Fleshman JW, et al. Fecal incontinence quality of life scale: quality of life instrument for patients with fecal incontinence. *Dis Colon Rectum.* 2000;43:9–16.

OPEN ACCESS Freely available online

PLOS | ONE

Hypoxia Imaging Endoscopy Equipped with Laser Light Source from Preclinical Live Animal Study to First-In-Human Subject Research

Kazuhiro Kaneko[1,2]*, Hiroshi Yamaguchi[3]*, Takaaki Saito[3], Tomonori Yano[1], Yasuhiro Oono[1], Hiroaki Ikematsu[1], Shogo Nomura[4], Akihiro Sato[4], Motohiro Kojima[5], Hiroyasu Esumi[6], Atsushi Ochiai[5]

1 Department of Gastroenterology, Endoscopy Division, National Cancer Center Hospital East, Kashiwa, Chiba, Japan, **2** Division of Science and Technology for Endoscopy and Surgery, National Cancer Center Hospital East, Kashiwa, Chiba, Japan, **3** Imaging Technology Center, FUJIFILM Corporation, Kaisei, Kanagawa, Japan, **4** Clinical Trial Section, National Cancer Center, Kashiwa, Chiba, Japan, **5** Department of Pathology, National Cancer Center Hospital East, Kashiwa, Chiba, Japan, **6** Research Institute for Biomedical Sciences, Tokyo University of Science, Noda, Chiba, Japan

Abstract

A goal in next-generation endoscopy is to develop functional imaging techniques to open up new opportunities for cancer diagnosis. Although spatial and temporal information on hypoxia is crucial for understanding cancer physiology and expected to be useful for cancer diagnosis, existing techniques using fluorescent indicators have limitations due to low spatial resolution and invasive administration. To overcome these problems, we developed an imaging technology based on hemoglobin oxygen saturation in both the tumor and surrounding mucosa using a laser endoscope system, and conducted the first human subject research for patients with aero-digestive tract cancer. The oxygen saturation map overlapped the images of cancerous lesions and indicated highly heterogeneous features of oxygen supply in the tumor. The hypoxic region of the tumor surface was found in both early cancer and cancer precursors. This technology illustrates a novel aspect of cancer biology as a potential biomarker and can be widely utilized in cancer diagnosis.

Citation: Kaneko K, Yamaguchi H, Saito T, Yano T, Oono Y, et al. (2014) Hypoxia Imaging Endoscopy Equipped with Laser Light ?Source from Preclinical Live Animal Study to
?First-In-Human Subject Research. PLoS ONE 9(6): e99055. doi:10.1371/journal.pone.0099055

Editor: Michael R Emmert-Buck, National Cancer Institute, National Institutes of Health, United States of America

Received March 24, 2014; **Accepted** April 17, 2014; **Published** June 10, 2014

Data Availability: The authors confirm that all data underlying the findings are fully available without restriction. All data are included within the manuscript.

Funding: This work was supported in part by the National Cancer Center Research and Development Fund (23-A-45) and (23-A-15) and the 3rd-term comprehensive 10-Year strategy for Cancer Control by the Ministry of Health, Labour and Welfare, and Accelerating Regulatory Science Initiative (H-24) [http://www.ncc.go.jp/en/index.html]. The funders had no role in study design, data collection and analysis, decision to publish, or preparation of the manuscript.

Competing Interests: H. Yamaguchi and T. Saito are employees of FUJIFILM Corporation. This technology has been developed to apply to an endoscope system. K. Kaneko has received grant support and a prototype endoscope system with hypoxia imaging function from Fujifilm Corporation, Tokyo, Japan. This does not alter our adherence to all the PLOS ONE policies on sharing data and materials.

* E-mail: kkaneko@east.ncc.go.jp (KK); hiroshi.mm.yamaguchi@fujifilm.com (HY)

Introduction

The cancer microenvironment is highly heterogeneous and hypoxia is strongly associated with the biological features of cancer [1]–[7]. Moreover, increasing evidence suggests that hypoxia is a critical component of cancer stem cell niche [8]. Thus, examinations into cancer hypoxia have been performed [9]–[11], but measurements having sufficient spatial-temporal resolution remain to be established.

Endoscopy is a suitable method for directly accessing the inside of the body and observing the cancerous lesion at high resolution. Therefore, an endoscope that can visualize the cancer microenvironment will open up new opportunities for cancer diagnosis and biological studies.

However, current methods, including fluorescent labelling techniques [12], [13] and hemoglobin absorption-based techniques [14]–[16], are limited in their applications to endoscope systems. In fluorescent labelling techniques, the spatial distribution of fluorescence is blurred because of a lack in specificity, low target accumulation, prolonged high retention and background, although improvements in agents continue to be made. In hemoglobin absorption-based techniques, many spectral images are required to detect the spectral differences between oxy- and deoxy-hemoglobin. Capturing variable wavelength images is time-consuming and the results are often blurred because the target does not remain in a state of rest under endoscopic observation.

Results

Development of hypoxia imaging technology

Herein, we developed an imaging technology that can derive the oxygen saturation (StO_2) images from small numbers of wavelength measurements. There were two challenges in deriving the StO_2 of the tissue in alimentary tracts from the differences in absorption spectra between oxy- and deoxy-hemoglobin using small numbers of wavelengths. First, the difference in optical absorption spectra in visible light region is small and the bandwidth between isosbestic points is very narrow. Second, reflectance of a tissue depends on hematocrit (Hct) as well as StO_2, because light absorption increases according to increases in hemoglobin density.

Selection of wavelength and bandwidth is vitally important in deriving StO_2 from small numbers of wavelength images. We found that a combination of narrow and two broad-band spectra are most suitable for derive StO_2 in alimentary tract tissue. (i) A narrow band at 473 nm was selected to detect the variations in StO_2, while the change in reflectance according to the variance in StO_2 at 473 nm is largest in the visible light region. We made the bandwidth very narrow (a few nanometres in width) to prevent a decrease in StO_2 sensitivity caused by wavelength width across the isosbestic points. (ii) A green broad-band was selected to detect variations in Hct. The green band is sensitive to variations in Hct because the absorption coefficient of hemoglobin is large. To make the signal robust to variations in StO_2, we broadened the green band (500–600 nm) across a few isosbestic points. (iii) A red broad-band was selected to detect the changes in illumination caused by the distance between the light exit window of the endoscope and the illuminated tissue. The red broad-band (600–700 nm) is robust to variations in StO_2 and Hct because the absorption coefficient of hemoglobin is small. We applied a computational technique to derive StO_2 signals from these three light signals. Briefly, the 473 nm signal and the green band signal are normalized against the red signal to cancel their dependence on illuminance. The normalized 473 nm signal is calibrated using the normalized green signal to cancel its dependence on Hct. Thus, pure StO_2 information can be obtained (Fig. 1A).

Based on these strategies, we developed an imaging system equipped with laser diodes of 445 and 473 nm and a white fluorescent pigment body. Broad-band diffused light is emitted from the white fluorescent pigment body excited by the 445-nm laser diode. The 473-nm diffused light, which is useful for illuminating narrow band light for StO_2 signals, is emitted by switching the laser light source from 445 nm to 473 nm. A color CCD sensor captures the 473-nm narrow band, and the green and red broad-band images (Fig. 1B).

In order to clarify the changes in quantity of light according to StO_2 and Hct, we introduced an intralipid phantom consisting of a

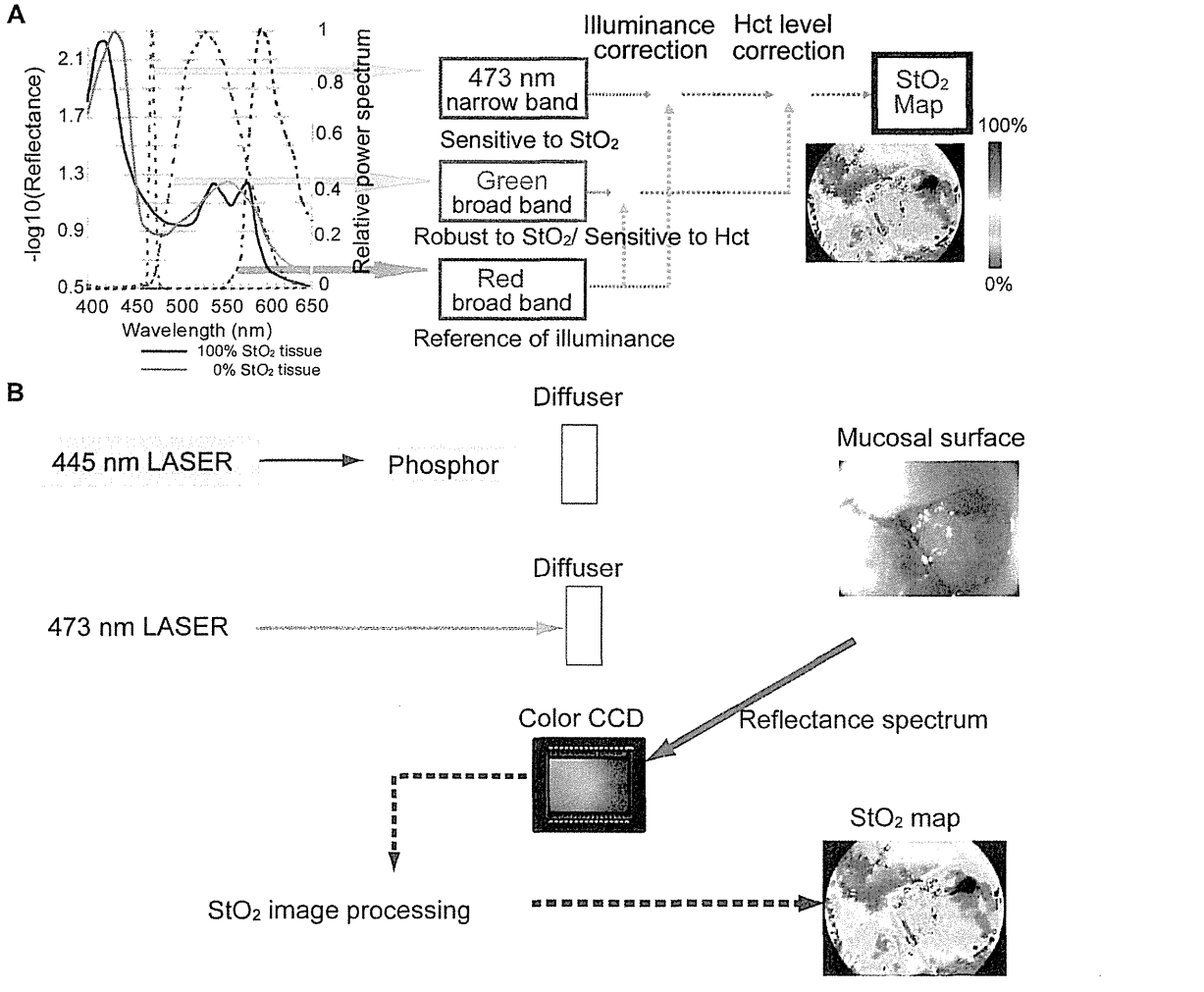

Figure 1. Mechanism of hemoglobin oxygen saturation imaging and schematic illustration of prototype endoscope system. (A) Illustration of the mechanism (see text for details.) (B) The 445-nm laser excited a phosphor equipped at the tip of the endoscope and emitted white light. The 473-nm laser light was emitted without the phosphor excitation. These two lights alternately illuminated the mucosal surface and the reflected lights were sequentially detected with a colour CCD in synchronization with light switching. The obtained images were processed and transformed into a StO_2 map.
doi:10.1371/journal.pone.0099055.g001

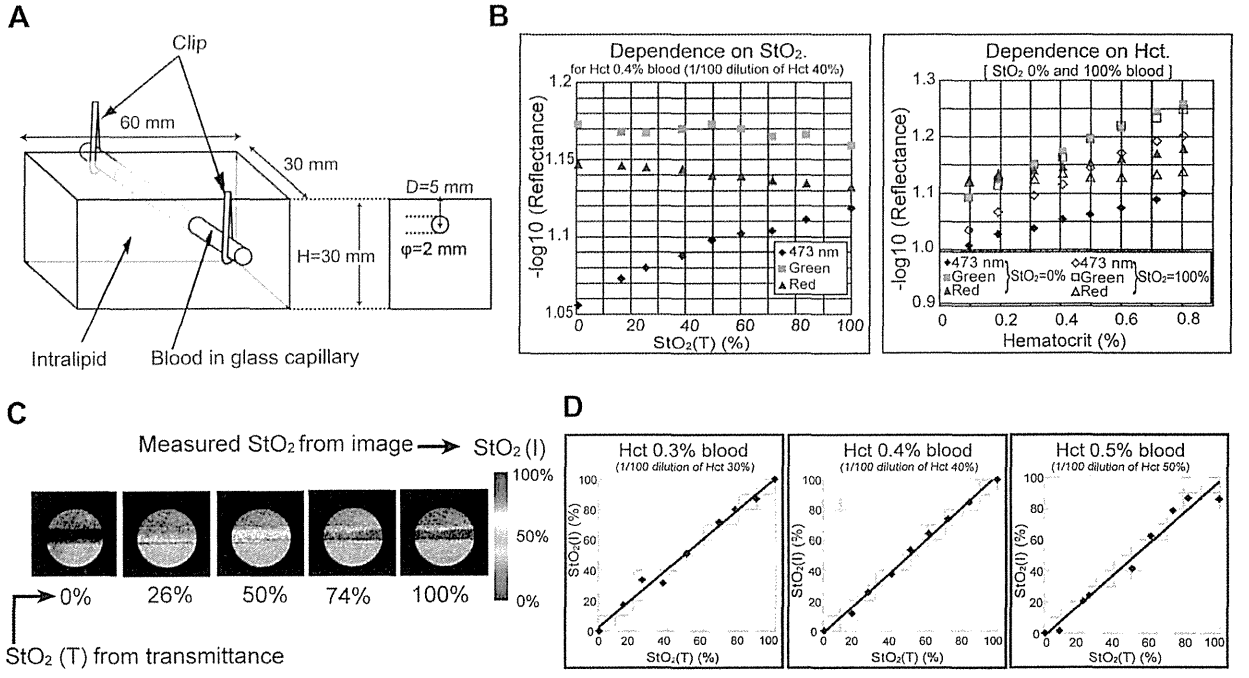

Figure 2. Verification of hemoglobin oxygen saturation imaging by observing a phantom. (A) Blood vessel phantom consisted of a glass tube filled with diluted blood and aqueous solution of intralipid. The intralipid solution strongly scattered incident light to simulate the living tissue around blood vessel. (B) The observed optical densities of the blood vessel at the three bands were dependent on StO2(T) (left) and Hct (right). Here, StO2(T) denotes the supposedly correct value of StO2 derived by analyzing the transmittance spectrum of blood. (C) StO2(I) map (derived by image processing) of the vessel. (D) Comparison of StO2(I) with StO2(T) (derived by measurement of transmittance spectra).
doi:10.1371/journal.pone.0099055.g002

glass capillary containing blood (Fig. 2A). The quantities of light as a function of StO_2 and Hct for 473 nm in the narrow, broad green and red bands were captured by the imaging system. Figure 2B shows that the 473 nm signal is sensitive to the change in StO2 and the green and red broadband signals are robust to that. Images were processed to create hemoglobin saturation maps. Figure 2C shows representative hemoglobin saturation pseudocolor maps of blood for different StO_2 levels. Measurements of hemoglobin saturation for different Hct levels derived with the imaging system corresponded well with the StO_2 measured using a spectral meter (Fig. 2D).

In vivo imaging of nude mouse transplanted with cancer cells

We then examined our approach using animal models. We used nude mice transplanted with A549 human cancer cells and attached window chambers [17] to the skin-peeled area, which kept the skin extended and enabled us to observe blood vessels under the skin. A549 cells were transplanted under the skin in the chambers (Fig. 3A). Three-band wavelength images using the imaging system to derive the StO_2 map from spectroscopic data were obtained (Fig. 3B left). The StO_2 map at 7 days after transplantation showed that the low StO_2 area was merged with the tumor-injected region where the tumor mass and aberrant tumor angiogenesis were augmented (Fig. 3B right). We confirmed the presence of cancer cells in histological images (Fig. 3C).

In vivo imaging of alimentary tracts with pigs

We then conducted an *in vivo* imaging experiment in pigs with a hypoxic area in the stomach tissue generated by transcatheter arterial embolization. Figure 4A shows a series of fluoroscopic images from the injection of the agent to embolization. Before embolization, high StO_2 value was observed (Fig. 4B lower left). Five minutes after embolization, the StO_2 map showed emergence of a hypoxic area corresponding to artificial vessel occlusion (Fig. 4B lower right). We also observed the change in StO2 at the esophagus. The StO2 was initially normal (around 70%) (Fig. 4C(i)). After the stomach removal, it declined to around 50–60% (Fig. 4C (ii)). The StO2 further dropped to near zero after the KCl injection (Fig. 4C (v)).

Human subject research

Next, we conducted a proof-of-the-concept research [18] for 40 patients with neoplastic lesions in the esophagus including the pharynx, stomach and colorectum (Table 1). In this first in human subject research (UMIN 000004983), two types of StO_2 images were used. One was a pseudocolor StO_2 image that showed StO_2 levels as different hues, and the other was a StO_2 overlay image that overlapped StO_2 levels in blue on a white light illumination image to detect background mucosa. Figure 5A shows an example of the StO_2 map for rectal adenocarcinoma. The hypoxic area was completely visible on the StO_2 map corresponding to the cancer region. Pathological diagnosis by H&E (hematoxylin and eosin) staining showed adenocarcinoma infiltrating into the submucosal layer (Fig. 5B upper). In this case, HIF1 alpha expression in immunohistochemical staining was found in the area described as hypoxic on the StO_2 map (Fig. 5B lower).

The hypoxic area was confirmed in early cancer. Eight colorectal adenomas with histological low-grade atypia were also detected as hypoxia, ranging between 3 mm and 10 mm in

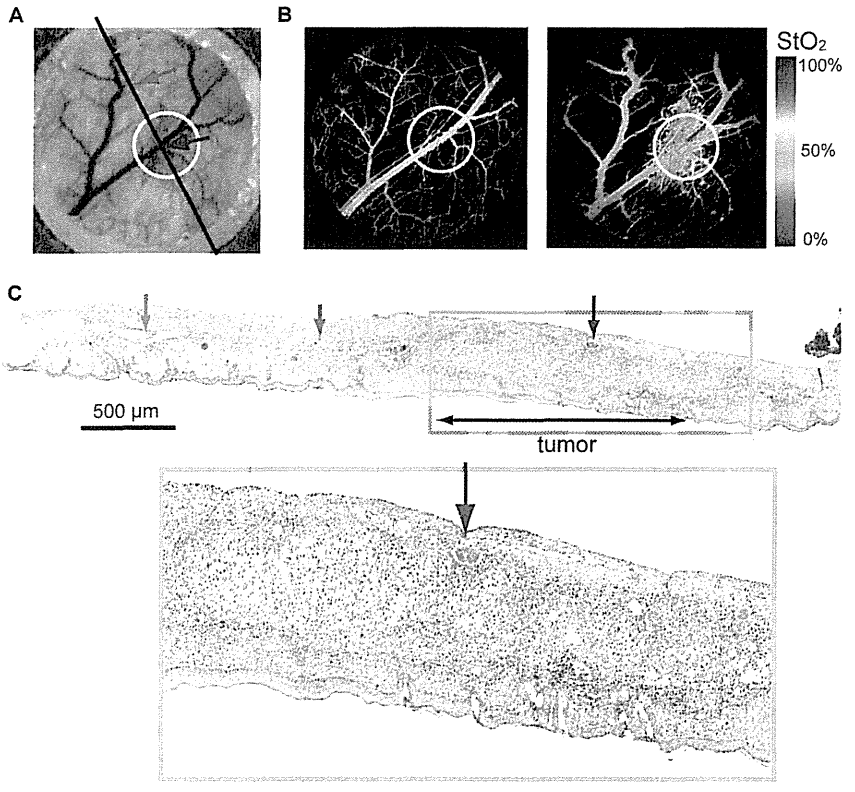

Figure 3. *In vivo* imaging of nude mouse implanted with cancer cells. (A) White light image of the mouse. The solid line corresponds to the cross-section of pathological assessment. (B) StO2 map of mouse before transplantation (left). Hypoxia developed at the tumor at 7 days after transplantation (right). (C) Histological picture (hematoxylin-eosin stained) of skin resected from the mouse at 14 days after transplantation (upper right, lower). Arrows indicate corresponding vessels.
doi:10.1371/journal.pone.0099055.g003

diameter (Fig. 5C upper, Video S1). Furthermore, one of the eight adenomas showed co-lesions combined with adenoma and hyperplasia. The low StO_2 region was detected in the adenoma portion, but not in the hyperplasic portion (Fig. 5C lower).

Figure 5D shows the observed StO_2 differences between neoplastic and non-neoplastic areas. Median StO_2 differences between neoplastic and non-neoplastic areas in the pharynx, esophagus, stomach and colorectum were −15.4%, −14.5%, −5.1% and −21.5%, respectively. There were significant differences in StO_2 levels between neoplastic and non-neoplastic areas in the esophagus ($p = 0.0078$ on Wilcoxon signed-rank test, 8 patients in each area ($n = 8$)) and colorectum ($p = 0.0001$, $n = 14$), but not in the stomach ($p = 0.9341$, $n = 15$) or pharynx ($p = 0.2500$, $n = 3$). Furthermore, sensitivity of neoplasia, defined as the proportion having correctly detected neoplasia, in the pharynx, esophagus, stomach, and colorectum was 67%, 100%, 33% and 86%, respectively.

Discussion

This is the first human subject research using the endoscopic hemoglobin oxygen saturation imaging technology for patients with aero-digestive tract cancers or adenomas. Before the human subject research, we evaluated our technology using a phantom and animals.

From the results of the phantom experiments, we confirmed that the green signal is useful for the separation of StO_2 and Hct information from the 473 signal. The characteristic that the red signal is robust to Hct and StO_2 is also important for the endoscopic application. The movement of the endoscope and alimentary tract tissue causes the change in illuminance during endoscopic observations. The robustness of red signal to Hct and StO_2 enables us to correct the change in illuminance.

Using dorsal skin-fold chamber mouse model, we detected temporal and spatial heterogeneity of oxygen saturation in tumor region. In a previous study [16], similar results were obtained using a hyperspectaral imaging system. The hyperspectral imaging system acquired images from 500 to 575 nm in 5-nm intervals to derive StO_2 map. We consider the hyperspectral imaging system needs long imaging times and a high-power source for sample illumination. Advantages of our technology in endoscopic application are short imaging times and the simplicity of the instruments. In *in-vivo* imaging experiments with pigs, we confirmed that our hypoxia imaging technology with endoscope can visualize the StO_2 map of alimentary tract tissue in real-time.

From the results of our human subject research, we can see that hypoxic imaging could clearly distinguish neoplasia from non-neoplasia in the esophagus and colorectum. As clinical benefits, screening of oesophageal and colorectal neoplasia, or prediction to efficacy of chemotherapy or radiotherapy can be utilized. Compared to the esophagus and colorectum, gastric cancer showed variations in tumor oxygen levels. Some cases exhibited hyperoxic conditions when compared with noncancerous areas around gastric cancer, but no significant differences were observed in

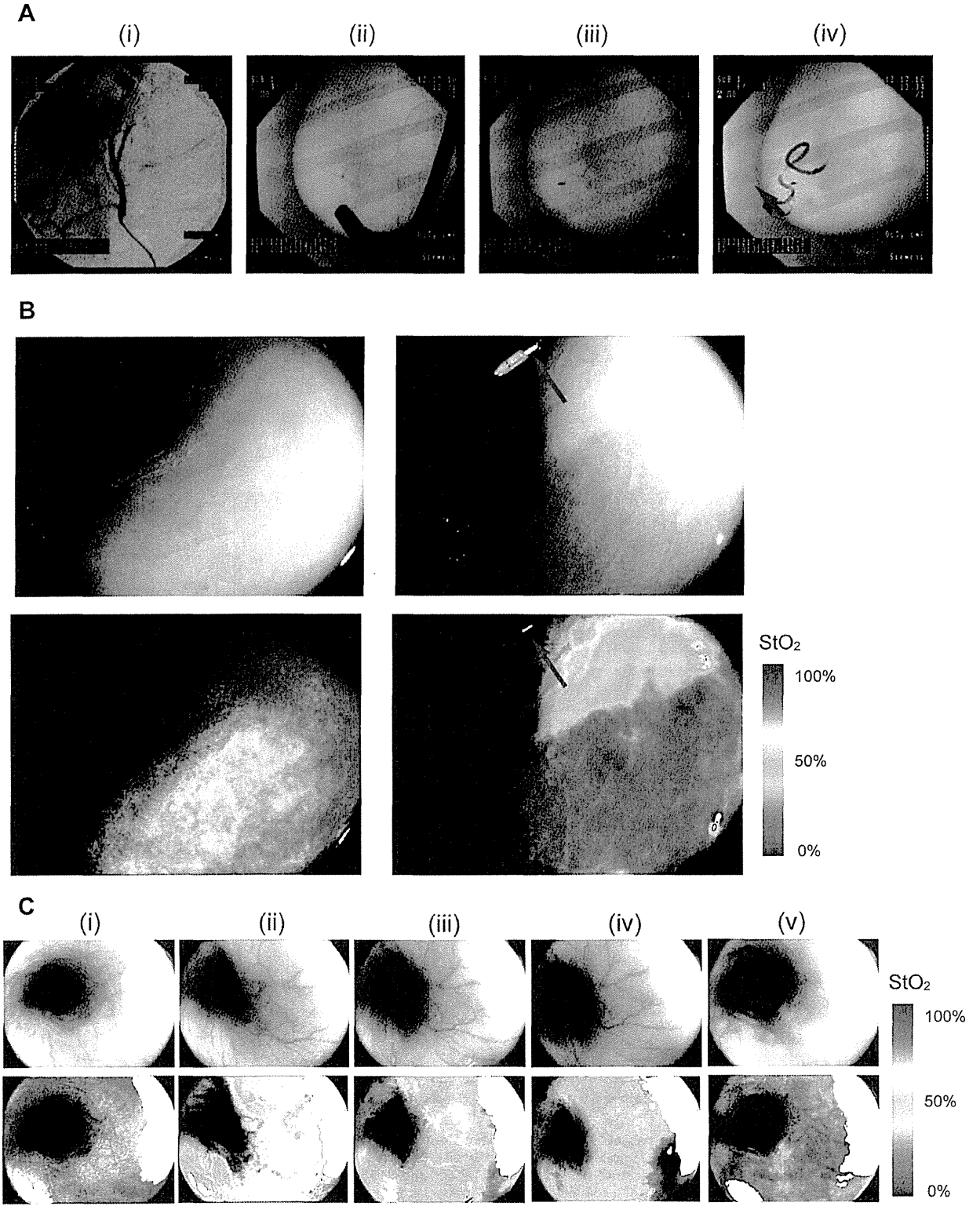

Figure 4. *In vivo* imaging with pig. (A) X-ray fluoroscopic images during application of transcatheter arterial embolization in pig stomach. (i) Image of the target vessel. (ii) Image of the endoscope inserted into the stomach. (iii) Red arrow indicates marking clip to identify the target area. (iv) Image of injected hystoacryl medium into the artery from the catheter. (B) White light images (upper) and StO_2 maps (lower) of the gastric mucosal surface visualized by laser endoscope system before embolisation (left) and five minutes after embolisation (right). (C) White light images (upper) and